TABLE 7.1

Dimensions of Example Magnetrons and a Comparison of the Operating Frequency Estimate from Equation 7.3, Valid Only for π-Mode Operation in Noninverted Magnetrons, with the Actual Operating Frequency

	f (GHz)	λ (cm)	r_c (cm)	r_c/λ	r_a (cm)	r_a/λ	r_v (cm)	f_π (GHz) Equation 6.3	f_π/f	h (cm)	h/λ
MIT A6,[a] 2π	4.6	6.5	1.58	0.24	2.1	0.32	4.11	na	—	7.2	1.11
MIT A6,[a] π	2.34	12.8	1.58	0.12	2.1	0.16	4.11	3.73	1.59	7.2	1.11
MIT D6[a]	4.1	7.3	1.88	0.26	2.46	0.34	4.83	na	—	1.88	1.15
MIT K8[a]	2.5	12.0	2.64	0.22	4.02	0.34	6.03	3.73	1.49	2.64	0.60
LLNL,[a] 2π	3.9	7.7	1.58	0.21	2.11	0.27	4.25	na	—	7.2	0.94
PI[b]	1.1	27.0	1.27	0.05	3.18	0.12	8.26	1.47	1.34	20	0.74
PI[c]	2.8	11.0	1.26	0.12	2.1	0.19	4.20	3.57	1.28	7.0	0.64
PI[d]	8.3	3.6	0.67	0.19	1.35	0.39	2.20	8.82	1.06	6.0	1.67
Inverted Magnetrons											
MIT M8[a]	3.7	8.1	4.26	0.526	2.9	0.358	1.28	na	—	5.1	0.59
MIT M10[a]	3.7	8.1	4.64	0.573	3.8	0.469	2.55	na	—	4.6	0.30
NRL[a]	3.2	9.4	21.3	2.27	19.4	2.06		na	—	5.1	0.54
SNL[a]	3.1	9.7	6.79	0.700	5.22	0.538	3.68	na	—	9.2	0.95

Note: Data are from the Massachusetts Institute of Technology (MIT), Lawrence Livermore National Laboratory (LLNL), Physics International (PI, now Titan Pulse Sciences Division), Naval Research Laboratory (NRL), and Sandia National Laboratories (SNL).

[a] Reference 14.
[b] Reference 16.
[c] Reference 17.
[d] Contact James Benford.

FIGURE 7.9
A rising-sun magnetron geometry with alternating anode cavity lengths. (From Lemke, R.W. et al., *Phys. Plasmas*, 7, 706, 2000. With permission.)

also show dimensions for four inverted magnetrons, for which $r_c > r_a$; we shall consider these later.

Mode competition is a serious issue in all microwave devices because each mode of an oscillator grows from the ambient noise of the Brillouin layer. The key to achieving high power is to avoid mode competition, and so to operate in a single mode. In the A6 magnetron, with only six cavities, the differences in frequency and azimuthal phase velocity, ω_n/n, are sufficiently large that mode competition can be avoided. Under different circumstances, for example, when more resonator cavities are added, more complex configurations, such as the *rising-sun* geometry (Figure 7.9),[18] create greater frequency separation between the π-mode and other modes, preventing mode competition*. We also note, as pointed out in the reference, that any configuration with alternating cavity characteristics constitutes a rising-sun magnetron, including coupling the output from every other cavity, even if the cavities are nominally of equal length.

Figure 7.10 is the dispersion relation for a rising-sun magnetron of the type shown in Figure 7.9.[13] For this device, $r_c = 7.3$ cm, $r_a = 9.7$ cm, $r_1 = 12.5$ cm, and $r_2 = 16.2$ cm; the 14 cavities all have the same angular width of about 10.3°. The dashed line is the dispersion curve for a 14-cavity magnetron with equal cavity depths of $r_d = (r_1 + r_2)/2 = 14.35$ cm. Note the effects of alternating the depths of the cavities. First, the periodicity of the structure is changed, with N = 7 identical pairs of cavities, rather than N = 14 identical individual cavities. Second, the n = 7 mode can now be regarded as either the π-mode of a 14-cavity set (with the fields reversing from one cavity to the next, without regard to its depth) or the 2π-mode of a 7-cavity set (with the fields in phase between cavities of the same depth). Third, the dispersion curve for the N = 14 magnetron is now split into two curves for the rising-

* Strapping, while a useful practice in conventional magnetrons, may well be impractical at high power due to breakdown problems.

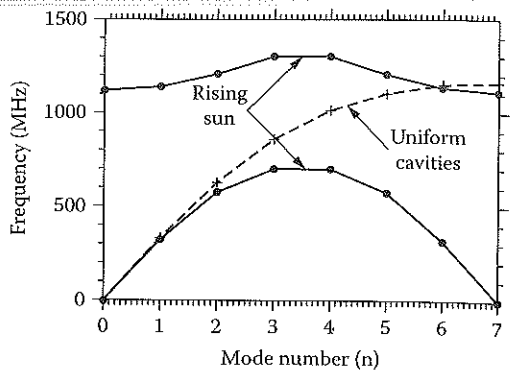

FIGURE 7.10
Dispersion relation for a rising-sun magnetron of the type shown in Figure 7.9, with the dimensions given in the text. (From Lemke, R.W. et al., *Phys. Plasmas*, 7, 706, 2000. With permission.)

sun magnetron; as $r_1 \rightarrow r_2$, the two rising-sun curves coalesce to form the single N = 14 curve. Simulations showed the upper n = 7 mode to provide the most efficient microwave generation. There is mode competition from the upper n = 6 mode; at large values of r_2/r_1, competition between the lower n = 3 and 4 modes becomes an issue also. In addition to this mode competition, there is also a zero-azimuthal-harmonic issue, which we will discuss in Section 7.5, that limits the output power.

7.3.2 Operating Voltage and Magnetic Field

As we stated earlier, for a given voltage, the applied magnetic field must be large enough to form the initial electron sheath around the cathode without allowing breakdown of the gap, but not so large that the rotational velocity of the electrons is too slow to allow resonance with the modes of the resonator formed by the coupled interaction space and anode cavities, as indicated by Equations 7.1 and 7.2.

As we discussed in Section 4.7, the critical magnetic field to prevent breakdown of the anode–cathode gap in the magnetron is the so-called Hull field (see Problem 8), which in the case of a purely axial field is given by[19]

$$B^* = \frac{mc}{ed_e}\left(\gamma^2 - 1\right)^{1/2} \tag{7.5}$$

where m and –e are the mass and charge of an electron, c is the speed of light,

$$\gamma = 1 + \frac{eV}{mc^2} = 1 + \frac{V\left(kV\right)}{0.511} \tag{7.6}$$

with V the anode–cathode voltage, and d_e the effective gap in cylindrical geometry,

$$d_e = \frac{r_a^2 - r_c^2}{2r_a} \tag{7.7}$$

When $B_z > B^*$, the electrons drift azimuthally within a bounded electron cloud called the Brillouin layer. As $B_z \rightarrow B^*$, the electron cloud extends almost to the anode. As the magnetic field increases, the cloud is confined closer and closer to the cathode. Remarkably, even though Equation 7.5 takes account of collective space-charge and diamagnetic effects from the electron layer, it is exactly the result one would obtain if one set the Larmor radius for a single electron equal to d_e.

In a magnetron, the electric field due to the applied voltage is predominantly radial, E_{r0}. The magnetic field is the sum of contributions from the externally applied axial field, modified by the diamagnetic effects of the azimuthal flow of electrons, and azimuthal components created by axial current flow in the cathode and radial current flow from the spokes. Current flows axially into the magnetron to support both axial current flow off the opposite end of the cathode to the wall at anode potential and radial current flow carried by the spokes in the anode-cathode gap. When flow off the end of the cathode is minimized, and when the azimuthal field from the axial current is relatively small, the magnetic field is predominantly axial. According to the left side of Equation 7.2, the drift velocity of an electron in this case is thus largely azimuthal, approximately given by E_{r0}/B_z, which decreases as B_z increases. Therefore, for a given voltage, there is some maximum B_z above which the electrons will be too slow to achieve resonance with the phase velocity of the electromagnetic wave supported by the anode structure. The relationship between the voltage and magnetic field at this threshold is called the *Buneman–Hartree condition*, which for a relativistic magnetron with an axial magnetic field, ignoring axial geometrical variations, is given by[19]

$$\frac{eV}{mc^2} = \frac{eB_z\omega_n}{mc^2 n} r_a d_e - 1 + \sqrt{1 - \left(\frac{r_a\omega_n}{cn}\right)^2} \tag{7.8}$$

In this expression, ω_n is the frequency in radians per second of the nth azimuthal mode. For a given voltage, this expression gives the maximum B_z for which high power output is expected; alternatively, it is the minimum V, given B_z, for high power operation (see Problems 9 and 10).

When the field from the axial current flow I_z becomes significant, the Buneman–Hartree condition for long cathodes is modified to

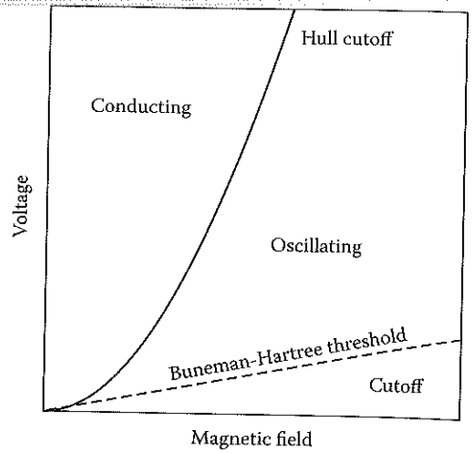

FIGURE 7.11
Magnetron operating domains in B_z-V parameter space.

$$\frac{eV}{mc^2} = \frac{eB_z\omega_n}{mc^2 n} r_a d_e - 1 + \sqrt{\left[1+b_\phi^2\right]\left[1-\left(\frac{r_a\omega_n}{cn}\right)^2\right]} \tag{7.9}$$

where

$$b_\phi = \frac{I_z(kA)}{8.5}\ell n\left(\frac{r_a}{r_c}\right) \tag{7.10}$$

This expression could also be modified to take account of contributions to b_ϕ in the event that the magnetic field component due to radial current flow became comparable to B_z in magnitude, although that contribution to the field will vary axially.

Figure 7.11 shows the operating domain of the magnetron in B_z-V parameter space. For a given voltage, if the magnetic field is too weak, electrons are allowed to cross the gap and breakdown occurs; if too strong, the oscillations are cut off. The space between the Hull cutoff requirement in Equation 7.5 and the Buneman–Hartree condition of Equation 7.8 or 7.9 is the region of oscillation. Efficient operation usually occurs just to the left of the Buneman–Hartree threshold.

7.3.3 Characteristics of Magnetrons

In operation, the interaction between the electrons and the microwave fields is highly nonlinear. The important parameters, which can be either determined empirically or predicted using computer simulation, are (1) the actual operating frequency; (2) the output power P; (3) the efficiency η, relating the pulsed power electrical input, $P_{PP} = VI$, to the microwave output, P; and (4) the parameter relating the operating current I to the voltage V.

To understand these and other magnetron parameters, consider Table 7.2, with a representative set of parameter values for operating relativistic magnetrons.[14,16,20] Note that most of the magnetrons in the table are truly relativistic, with operating voltages above 500 kV. The operating current spans a broad range, with associated impedances running from just over 10 Ω to several hundred ohms. Similarly, the applied magnetic fields span a broad range, from 0.2 T to about 1 T or slightly higher. Several of the devices generate output power at the level of several gigawatts. Efficiencies of about 30%, or perhaps more, can be reached. Some of the magnetrons are inverted, with $r_a < r_c$. The NRL magnetron is an outlier with respect to size, being much larger than the other devices.

The actual operating frequency will be somewhat lower than the cold-structure frequency discussed in Section 7.3.1. A good example is the MIT A6 magnetron,[8] for which the calculated and measured cold frequencies for the π- and 2π-modes were compared to the hot frequency with electrons, as shown in Table 7.3. The agreement between the calculated and measured cold frequencies is better than 3%, consistent with the fact that the anode length of 7.2 cm is somewhat longer than the free-space wavelength of the 2π-mode, and more than half that of the π-mode, so that the underlying assumption of an infinitely long anode holds.

The microwave output power P is proportional to the electrical power into the device, which is the product of the voltage, V, and the current, I, with the efficiency η the proportionality constant:

$$P = \eta VI \tag{7.11}$$

The impedance Z is the ratio Z = V/I, so that one can write

$$P = \eta\frac{V^2}{Z} \tag{7.12}$$

(See Problems 1 and 12.)

Experimental evidence from four different magnetrons operating over different frequency ranges between 1.07 and 3.23 GHz, at voltages between 220 and 500 kV, indicates that P scales with magnetron voltage V as V^m, with m lying between 2.46 ± 0.35 for one device and 2.74 ± 0.41 for another.[21] Thus, for nonrelativistic voltages V < 500 kV, if η is approximately constant, Equation 7.11 indicates that in those magnetrons

$$I \approx KV^{3/2},\ \text{V} < 500\ \text{kV} \tag{7.13a}$$

TABLE 7.2

Selection of Experimental Results for Magnetrons

	f (GHz)	V (MV)	I (kA)	Z = V/I (Ω)	B (T)	P (GW)	t (nsec)	E (J)	η (%)	N	Mode
MIT A6[a]	4.6	0.8	14	57	1.0	0.5	30	15	4	6	2π
MIT D6[a]	4.1	0.3	25	12	0.49	0.2	30	6	3	6	2p
MIT K8[a]	2.5	1.4	22	64	0.54	0.05	30 [b]	1.5	0.2	8	p
LLNL[a]	3.9	0.9	16	56	1.6	4.5	16	72	30	6	2π
SRINP 1[b]	2.4	1.1	4	275	1.2	2.0	50	100	45	6	p
SRINP 2[b]	2.4	0.45	6	75	0.4	0.8	300	240	30	6	p
IAP 1[b]	9.1	0.6	7	86	0.6	0.5	20	10	12	8	p
IAP 2[b]	9.2	0.95	40	24	1.0	4.0	15	60	11	8	p
PI[c]	1.1	0.8	34	24	0.85	3.6	10	36	13	6	p
PI[b]	2.8	0.7	20	35	1.0	3.0	20	60	20	6	p
PI[b]	8.3	1.0	30	33	1.0	0.3	10	3	0.1	6	p
Inverted Magnetrons											
MIT M8[a]	3.7	1.7	4	425	0.46	0.4	30	12	12	8	p
MIT M10[a]	3.7	1.6	9	178	0.7	0.5	30	15	3	10	p
NRL[a]	3.2	0.6	5	120	0.25	0.5	30	15	17	54	p
SNL[a]	3.1	1.0	10	100	0.3	0.25	50	12	3	12	p

Note: Data are from the Massachusetts Institute of Technology (MIT), Lawrence Livermore National Laboratory (LLNL), Scientific-Research Institute of Nuclear Physics in Tomsk, Russia (SRINP), Institute of Applied Physics in Nizhny Novgorod, Russia (IAP), Physics International (PI; now L3 Communications Pulse Sciences), Naval Research Laboratory (NRL), and Sandia National Laboratories (SNL). The parameters in the columns are, from left, the frequency, voltage, current, impedance, magnetic field, output power, pulse length, energy per pulse, efficiency, number of cavities in the anode, and operating mode.

[a] Reference 14.
[b] Reference 20.
[c] Reference 16.

TABLE 7.3

Comparison of the Calculated and Measured Cold Frequencies for the π- and 2π-Modes of the A6 Magnetron to the Hot Frequency with Electrons[8]

	π-Mode	2π-Mode
Calculated cold frequency (GHz)	2.34	4.60
Measured cold frequency (GHz)	2.41	4.55
Measured hot frequency (GHz)	2.3	4.6

$$P \approx \eta K V^{5/2}, \text{ V} < 500 \text{ kV} \tag{7.13b}$$

which is the form we would expect for a nonrelativistic Child–Langmuir diode (see Section 4.6.1), with K known as the perveance. This result is surprising in that the electron flow in magnetrons is strongly influenced by the magnetic field, whereas the flow in a Child–Langmuir diode, which has no axial magnetic field, is assumed to be purely radial. The data suggest that the radial current transport in a magnetron enabled by the microwave fields is limited by the space charge in the spokes.

Let us look more closely at the current flow in a magnetron, which occurs despite the fact that the axial magnetic field lies above the critical Hull field for insulation given by Equation 7.5. To see this, compare the normalized current-B_z plot for the smooth-bore magnetron, which has a constant-radius anode with no cavities, of Figure 7.12[22] with the plots of current and voltage vs. B_z for the A6 in Figure 7.13.[8] With a smooth anode, the microwave signal level within the anode–cathode gap is very small and the current, which is normalized to the Child–Langmuir value for $B_z = 0$, drops to a negligible level as the magnetic field is increased to B^*. The solid curve in Figure 7.12 is a theoretical value, while the data points are drawn from configurations with a number of different gap values, $r_a - r_c$. Qualitatively, the drop in the solid curve and the data as B_z increases is the result of increased travel time across the gap caused by the curving of the electron trajectories by the magnetic field. The deviation of the data from the theory is largely the result of the fact that an axial current flows in the cathode to support the radial current, and this axial current creates an azimuthal magnetic field component that modifies the total magnetic field.

The plot of current vs. B_z in Figure 7.13 for an A6 magnetron with anode cavities shows the effect of the strong microwave fields in the device. As the magnetic field increases above $B^* = 4.9$ kG (0.49 T) for the given voltage and gap, the current does not drop to zero, but rather declines continuously with B_z. This is not to say that the constraint $B_z > B^*$ is irrelevant in a magnetron or CFA, but rather that, in operation, current is carried by the nonequilibrium spoke structures.

The plot of power vs. B_z for the A6 shown in Figure 7.14 shows how sharply the power peaks at the optimum B_z of about 0.76 T, where the output

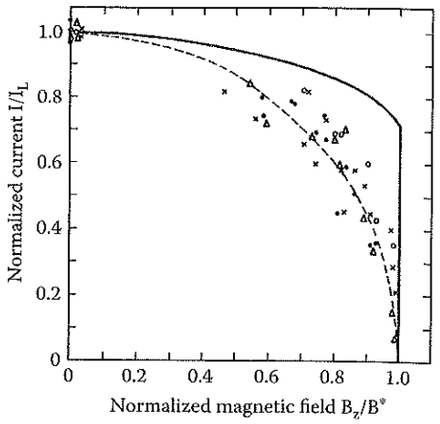

FIGURE 7.12
Current normalized to the Child–Langmuir value for $B_z = 0$, I_L, in a smooth-bore magnetron. The solid curve is a theoretical calculation ignoring the current flow in the cathode, and the data points were taken for a number of different anode–cathode gaps. The dashed curve is a quadratic fit to the data. (From Orzechowski, T.J. and Bekefi, G., *Phys. Fluids*, 22, 978, 1979. With permission.)

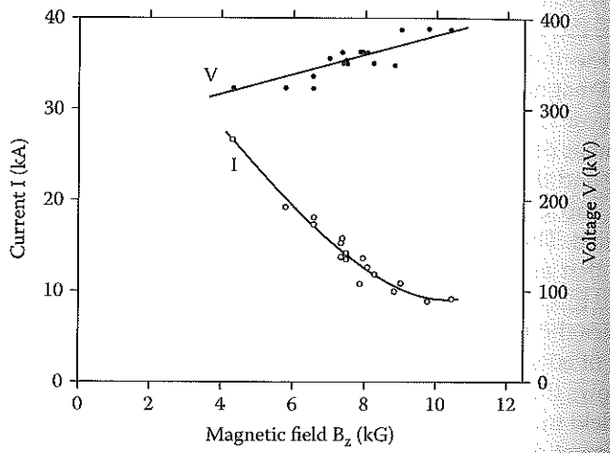

FIGURE 7.13
Current and voltage vs. B_z in the MIT A6 magnetron. (From Palevsky, A. and Bekefi, G., *Phys. Fluids*, 22, 986, 1979. With permission.)

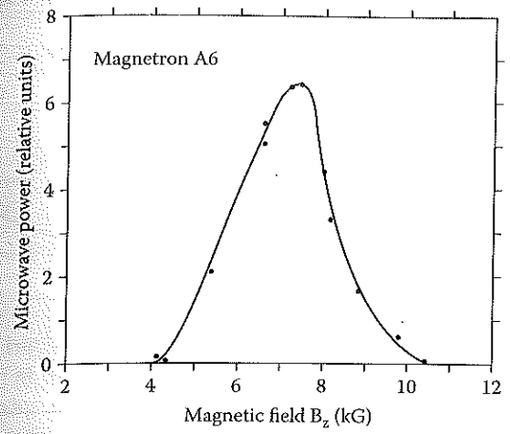

FIGURE 7.14
Output power vs. B_z in the MIT A6 magnetron. (From Palevsky, A. and Bekefi, G., *Phys. Fluids*, 22, 986, 1979. With permission.)

is about 900 MW. The range of operating parameters' regime for the A6 is shown against the Hull and Buneman–Hartree curves in Figure 7.15. The magnetic fields approximately span the region between the Hull cutoff criterion of Equation 7.5 and the Buneman–Hartree condition of Equation 7.8 for the 2π-mode, and the peak power occurs close to the Buneman–Hartree condition. Computer simulations of the A6 indicate that, for the lower-frequency π-mode, as B_z increases, the most efficient operating voltage shifts upward from the Buneman–Hartree voltage.[13] This is because the sheath is too narrow at the Buneman–Hartree voltage and couples poorly to the microwaves; at higher voltages, the sheath becomes thicker and couples more efficiently.

7.3.4 Summary of Magnetron Design Principles

One can scope out many of the basic parameters of a magnetron using the expressions in this chapter. With the dispersion relation derived using the procedure in the reference, we can find the expected operating frequency for a desired operating mode, given the cathode and anode radii and the geometrical parameters of the cavities. With the mode number and frequency in hand, we can find the operating region in V-B_z parameter space using the Hull insulating and Buneman–Hartree criteria. The optimal voltage for a given magnetic field will be close to, but above, the Buneman–Hartree voltage, rising farther above that voltage as the magnetic field increases. If we wish to predict the impedance (or, at lower voltages, perveance), efficiency, and output power in advance of an experiment, we must either work empirically, perhaps making small excursions from known designs and measuring

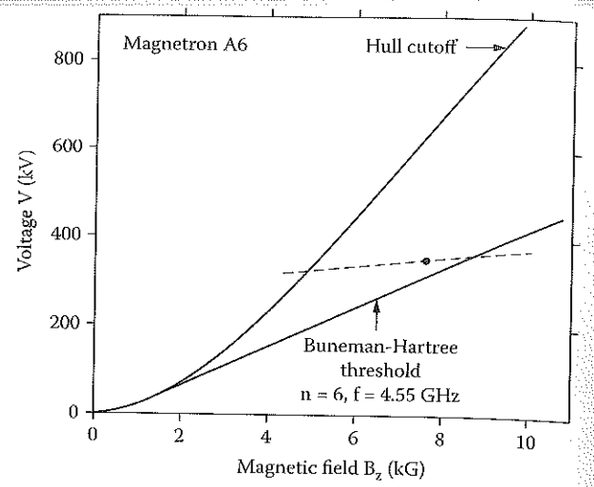

FIGURE 7.15
Buneman–Hartree diagram for the 2π-mode (N = 6) in the MIT A6 magnetron. The solid dot is the peak power operating point, and voltages at which maximum power is achieved at a given magnetic field between about 0.4 and 1.0 T (4 to 10 kG) are shown along the dashed curve. (From Palevsky, A. and Bekefi, G., *Phys. Fluids*, 22, 986, 1979. With permission.)

the resulting currents, or employ a simulation that is normalized to experiment. Nevertheless, we know that the impedance will be within a factor of two of about 100 Ω, and an efficiency of perhaps 20 to 30% can be attained, from which we can predict an expected output power.

7.4 Operational Features

Table 7.4 compares the typical operating parameters for conventional and relativistic magnetrons. Conventional pulsed, high power magnetrons typically operate at power levels up to about 5 MW, although a 60-MW rising-sun magnetron was built with conventional technology.[23] Voltages and currents in 5-MW conventional magnetrons are typically 50 kV or less and about 200 A or slightly more, so that impedance $Z \sim 200$ to 250 Ω and perveance* $K \sim 20 \times 10^{-6}$ A/V$^{3/2}$; the 60-MW magnetron, by comparison, with a secondary-emission dispenser cathode, operated at about 120 kV and 800 A, so that $Z \approx 150$ Ω and the perveance was about the same as other conventional magnetrons. Referring back to Table 7.2, voltages in relativistic magnetrons are about an order of magnitude higher, and currents are one to two orders

* Perveance is many times expressed in units of pervs, with dimensions of A/V$^{3/2}$, or micropervs (= 10^{-6} pervs).

TABLE 7.4
Typical Operating Parameters for Conventional and Relativistic Magnetrons

Parameter	Conventional Magnetrons	Relativistic Magnetrons
Voltage	100 kV	500 kV
Current	~100 A	5–10 kA
Cathode process	Thermionic and secondary emission	Explosive emission
Pulse duration	~1 μsec	~100 nsec
Rise time	200 kV/μsec	~100 kV/nsec
Power	10 MW	~1 GW
Efficiency	~50%	~20–30%

of magnitude higher, with impedance ranging more broadly from 30 Ω upward, which at the lower end matches well with pulsed power machines. Besides the order of magnitude difference in operating voltage, the key difference is the much larger operating currents of relativistic magnetrons, which are enabled by the explosive emission mechanism from cold cathodes. Unfortunately, explosive emission creates a cathode plasma, and the motion of this plasma causes gap closure at velocities typically greater than 1 cm/μsec, limiting pulse lengths to something on the order of 100 nsec in the absence of special measures. In conventional magnetrons, on the other hand, pulse lengths are typically limited by anode heating. Consistent with the higher operating voltages and currents, relativistic magnetrons operate around 1 GW, about 100 times higher than conventional magnetrons, even given their lower efficiencies.

In the previous section, we discussed the theoretical design considerations in choosing, for example, the dimensions of the cathode and anode structure and the operating voltage and magnetic field. Here, we discuss the operational considerations for several situations: single fixed-frequency magnetrons, tunable magnetrons, repetitively operated magnetrons, and, for magnetron-based facilities, notably Orion, a transportable container-based facility for outdoor microwave effects studies.

7.4.1 Fixed-Frequency Magnetrons

The cross section of a typical relativistic magnetron is shown in Figure 7.16.[24] The magnet coils, along with the high-voltage electrical feed from the bottom of the figure, dominate the volume and mass of the magnetron itself. Experimental magnetrons have employed pulsed field coils, but water-cooled or superconducting magnets are needed in repetitively fired magnetrons operating at high average powers. Operation with permanent magnets might be possible, but there are no publications to date on this.

Operationally, the cathode must be built to promote the process of explosive emission, with the rapid and uniform production of the surface plasma that provides the high current densities — of the order of kA/cm^2 — required for space-charge-limited current flow in the radial direction. In addition, the

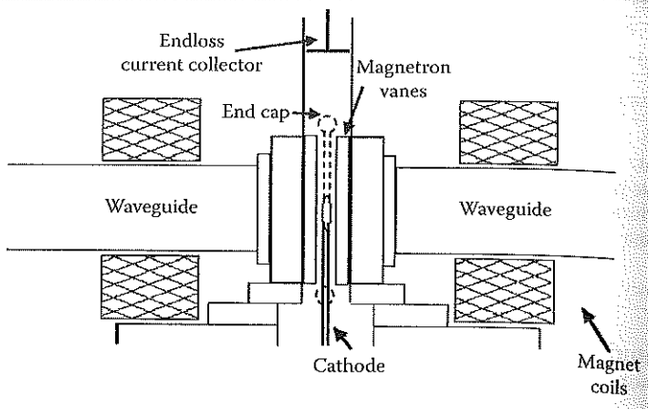

FIGURE 7.16
Cross section of a typical relativistic magnetron. The power feed is at the bottom of the picture. The cylindrical axis of the magnetron runs along the cathode stalk, and the magnet coils encircle the axis. (From Lopez, M.R. et al., *IEEE Trans. Plasma Sci.*, 30, 947, 2002. With permission.)

cathode must be designed to maximize the ratio of radial to axial current flow, since axial electron flow does not contribute to microwave generation. A number of cathode materials and configurations have been explored; these materials are placed on the cathode stalk at the slight bulge shown in the center of the magnetron in Figure 7.16. Placing a washer, or washers, with its sharp edges in the mid-section of the resonator increased power by as much as an order of magnitude, as was originally shown by Craig et al.[25] and quantified by Benford et al.[17] More recently, Saveliev et al. conducted a systematic investigation of magnetron cathodes comparing the performance of (1) smooth cylindrical cathodes with a variety of surfaces — velvet covered by a stainless steel mesh, carbon fabric, a stainless steel mesh, or plain stainless steel; (2) carbon fiber discs; and (3) pins.[26] They found substantial variation in relativistic magnetron performance among the different cathodes. In terms of peak power and energy per pulse, the cathode material that promoted the most uniform emission — velvet covered by a stainless steel mesh — was the best performer. Unfortunately, velvet cathodes evidenced considerable damage after 1000 shots, even though performance was still acceptable. The authors judged that stainless steel mesh without the velvet provided a better compromise between lifetime, power, and energy per pulse.

Although Phelps eliminated axial end loss in an early experiment by feeding electrical power to the cathode from both ends,[27] the more common approach has become the use of the *end caps*, shown in Figure 7.16. Note from the figure that the end caps are rounded, to reduce the electric fields at their surfaces. In experiments, the end caps may be coated with glyptal, a substance that inhibits electron emission; unfortunately, glyptal coatings are easily damaged and must be replaced rather frequently. Saveliev et al. showed that end caps almost doubled the efficiency, to 24% in an L-band rising-sun magnetron operating at over 500 MW.[26] Lopez et al. similarly found that the use of end caps reduced the axial current loss from 80% of the total magnetron current to as little as 12% in a variant of the A6 magnetron[24] with an aluminum cathode coated with glyptal, except at the mid-section of the resonator, where 1-mm carbon fibers were glued to the cathode. Double end caps play additional desirable roles, defining the mode structure, suppressing axial mode competition, and maximizing the electric field in the mid-section of the resonator. As a final point, remember that axial current flow cannot be eliminated, since the axial current flow completes the circuit for the radially directed current in the spokes and since that current flow creates an azimuthal magnetic field and an axial $E_r \times B_\theta$ electron drift; however, axial flow off the end of the cathode, beyond the circuit including radial spoke flow, is a loss and should be suppressed.

Extraction of microwaves from relativistic magnetrons employs two rather different techniques. The most commonly used is *radial extraction* from the ends of one or more of the anode cavities into the fundamental mode of the output waveguide. Sze et al.[28] measured the effect of extraction through multiple ports. In their experiments, frequency did not depend upon the number of extraction ports and mode shifting did not occur. However, there was an optimum number of waveguides. Figure 7.17 shows that the maximum power from the A6 magnetron was obtained most easily with three waveguides, although six gave the same power. Power per waveguide declined steadily as the number of waveguides increased to four, and then was roughly constant. The cavity Q was reduced as more openings were

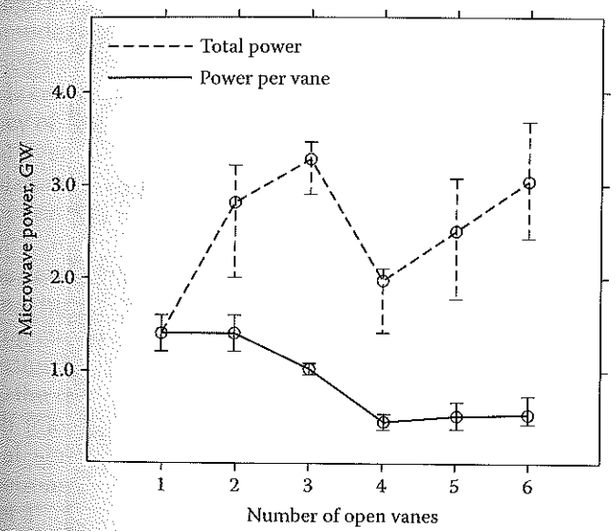

FIGURE 7.17
Power extracted from a six-vane A6 magnetron at Physics International as a function of the number of vanes. (From Sze, H. et al., *IEEE Trans. Plasma Sci.*, PS-15, 327, 1987. With permission.)

made in the resonator. Radio frequency (RF) field declined with Q, and the trade-off between cavity RF field and output power was optimized with three output resonators. We note that extraction from every other vane effectively creates a rising-sun configuration.[18]

Axial extraction of microwave power has also been used with two variations. Ballard et al. extracted from a magnetron with inverted polarity by using a downstream mode converter.[29] Kovalev et al.[30] tapered the magnetron resonator structure in the axial direction to merge with an output waveguide using a method called *diffraction coupling* in Russian works, making a gradual transition from the RF impedance of the magnetron to free-space impedance, as shown in Figure 7.18. In this 9.1-GHz magnetron with an eight-cavity anode, they claimed an output power in excess of 500 MW at 13 to 15% efficiency. Benford and Sze directly compared axial and radial coupling in another X-band magnetron.[31] Their six-vane magnetron was about two vacuum wavelengths long and suffered from axial mode competition. Using radial coupling, they were able to obtain reproducible operation when coupling from only one cavity; with coupling from more cavities, the power level was unstable. With axial coupling using a technique similar to that of Kovalev et al., they were able to raise the efficiency from less than 1% with radial coupling to more than 2%, with stable output power in excess of 350 MW. Figure 7.18 shows the anode of their magnetron, with the vane structure preserved in the flaring axial extraction region.

The radiation patterns for the radial and axial extraction methods differ substantially because each radiates different modes. Radial extraction in rectangular waveguide produces TE_{10} radiation patterns. The power distribution is smooth and linearly polarized. Axial extraction gives TM_{np}, where n is the azimuthal mode number and p is the radial index. Such patterns all have central nulls and therefore are unattractive. Mode converters might be used to convert to a more useful pattern.

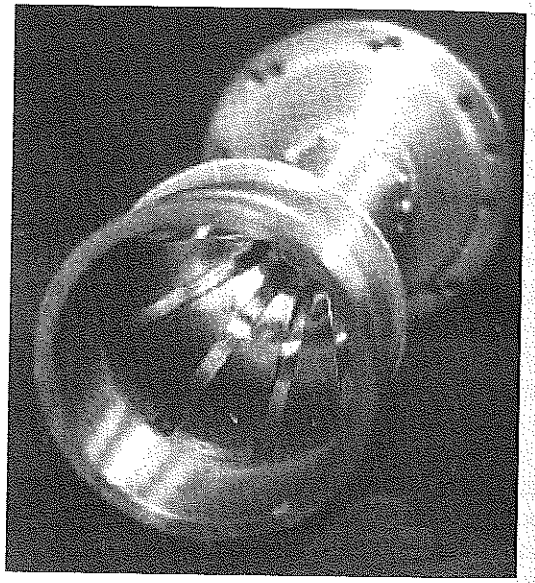

FIGURE 7.18
Axial extraction from a tapered resonator.

Figure 7.16 does not show the diagnostics that would be used in experimental devices and perhaps in some more mature systems. Total current into a magnetron is diagnosed with a Rogowski coil placed in the outer wall encircling the cathode stalk before it enters the magnetron resonator. A second Rogowski coil in the other wall downstream of the cathode end cap would be used to measure axial current loss. Directional couplers are used for power measurements, heterodyne and homodyne systems for frequency and bandwidth, and phase discriminators for phase relations. Close et al. measured the electric field in an evacuated waveguide extracted from the A6 by observing Stark broadening of the hydrogen Balmer line.[32] The result was 100 kV/cm, precisely that deduced from power measurements. Smith et al. measured the phase difference between adjacent resonators directly using a phase discriminator.[33]

7.4.2 Tunable Magnetrons

Mechanically tunable magnetrons require the physical modification of one of the key design parameters. In an initial exploration of mechanical tuning, Spang et al.[34] showed that the variation of the cathode radius of a variant of the A6 design allowed a rather broad frequency range of operation: operating in the 2π-mode, cathode radii varying from about 0.54 to 1.52 cm resulted in frequencies between about 4 and 4.6 GHz, a tunable range of 7% about the 4.3-GHz center frequency. At 4.6 GHz, the peak power was 700 MW with an efficiency of 15%. The π-mode frequency also varied slightly with cathode radius, but over a much reduced range (see Problem 11). Unfortunately, the actual replacement of the cathode was required in these experiments.

The adoption of a rising-sun geometry enabled the construction of a magnetron that can be tuned from shot to shot in a repetitively fired system. Prior to the development of tunable magnetrons, several groups investigated narrowband, high power rising-sun magnetrons. Treado et al. operated a 14-cavity rising-sun magnetron at 60 MW based on conventional technology.[23] When injection locked to a lower-power magnetron to stabilize the operating frequency, the 60-MW magnetron had a bandwidth of about 800 kHz, full width/half maximum (FWHM) about the center frequency of 2.845 GHz. Lemke et al. simulated the operation of 14- and 22-cavity relativistic rising-sun magnetrons.[18]

Levine et al. developed a family of high power, mechanically tunable, 10-resonator rising-sun magnetrons operating in the L- and S-bands.[35] The remarkable anode structure, shown in Figure 7.19, was made from a single piece of stainless steel by electron discharge machining. Without the joints

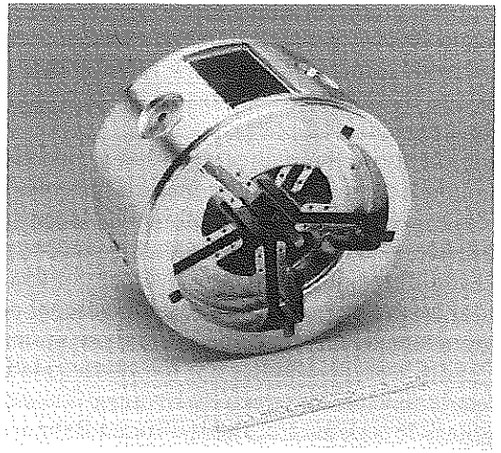

FIGURE 7.19
Anode structure for the mechanically tunable rising-sun magnetron. (Courtesy of L-3 Communications Pulse Sciences, formerly Physics International.)

and cracks of a device assembled from separate pieces, and using ceramic insulators and cryopumps in the vacuum system, the magnetron can be pumped down to 10^{-8} torr after it has been cleaned and vacuum baked. Note that the vanes are arranged in five closely spaced pairs. Tuning is effected by moving a sliding short in the narrow cavities with parallel walls, varying the depth of those cavities; that variation in depth, which changes the frequency of the device, requires a corresponding adjustment of the magnetic field. In the figure, we can see the circular holes in the outside of the anode block, through which the pins that push the tuning shorts pass. The tuning range for the L-band magnetron is approximately 24% about a center frequency of 1.21 GHz, while that for the S-band magnetron is 33% about a center frequency of 2.82 GHz. One of two extraction ports is seen in the top of the anode block in Figure 7.19. Extraction is thus from cavities with nonparallel walls. Arter and Eastwood's simulations show that the output power remains approximately the same even when additional extraction ports are added.[36]

7.4.3 Repetitive High-Average-Power Magnetrons

The original single-shot experiments with relativistic magnetrons were conducted with the aim of exploring basic physics and engineering issues. In shifting to repetitive operation, one must address several additional engineering and physics issues. On the engineering end, one must provide adequate prime power and the requisite magnetic field on either a continuous or pulsed basis. Further, one must design the pulsed power to provide high voltage and current at the required switching rates. With regard to prime power, we note that the important parameters are the duty factor for the pulsed power, D_{PP}, and the overall system efficiency from prime power to microwave output, η_{SYS}. The duty factor is

$$D_{PP} = R\tau_{PP} \tag{7.14}$$

where R is the repetition rate and τ_{PP} is the pulse length for the pulsed power on each shot. Note that Equation 7.14 involves τ_{PP}, rather that the microwave pulse length τ, highlighting the waste created by pulse shortening, which reduces the length of the output pulse relative to τ_{PP}. The overall system efficiency is a product of the efficiencies for the prime and pulsed power, microwave generation and extraction, and the antenna. For a radiated power P, the required prime power is

$$P_{PRIME} = \eta_{SYS} D_{PP} P = \eta_{SYS}\, R\tau_{PP}\, P \tag{7.15}$$

Given that η_{SYS} is the product of several efficiencies, even for magnetron efficiencies of 30 to 40%, the system efficiency could be a few percent.

From the standpoint of magnetron physics, two primary issues for repetitive operation are diode recovery and electrode erosion. The process of explosive emission and the deposition of electron energy in material surfaces release plasma and neutral particles that must clear the system between pulses. Systems must be clean, operating at high vacuum, to limit the surface contaminants that facilitate plasma formation, explaining the use of single-piece anodes, cryopumps (with sufficient pumping speed), and ceramic insulators in the previous subsection.

The second major issue in repetitive operation is electrode erosion. Pin and fiber-enhanced cathodes with longer lifetimes have been developed, but anode erosion is an intrinsically challenging issue in magnetrons, since electron deposition must occur within the cavity (see Problem 7). At high average power levels, water cooling of the anode and the collection surface for axial electron loss is required. To see this, consider the example of anode erosion, since most erosion is observed on the anode. A rough estimate of the magnitude of the erosion problem is that the peak dose for 700-keV electron deposition in most refractory metals is 6 (cal/g)/(cal/cm^2). Using S-band magnetron parameters as an example, a single 60-nsec electrical pulse for which 5 kA of electron current strikes 50 cm^2 of anode produces a surface heat increase of 6 cal/g. Neglecting conduction and radiation, we estimate that the heat of fusion will be exceeded in about 10 shots; ablation will occur thereafter.

Two U.S. industrial firms, GA[37] and AAI,[34] operated magnetrons at 1- to 2-Hz repetition rates for long periods, generating thousands of pulses. The latter used water-cooled vanes, a repetitively fired Marx bank, and pulsed conventional magnets. Intended for operation at a 10-Hz rate, it was limited to 2 Hz by unexpectedly high power demand in the magnets due to eddy current losses in the magnetron structure. In their 4.6-GHz A6 variant operating in the 2π-mode, there was noticeable anode vane erosion at 5000 shots, but no degradation in performance. The metal cathode, however, had to be